



# Interpreting the formation mechanism of a complex landslide: a case study of a reactivated landslide of a reinforced embankment slope

Qiuxiang Huang<sup>1,2</sup> · Jialin Wang<sup>1</sup> · Pinnaduwa H.S.W. Kulatilake<sup>2</sup> · Haofeng Guo<sup>1</sup> · Jipeng Shen<sup>1</sup>

Received: 27 April 2023 / Accepted: 17 November 2023 / Published online: 1 December 2023  
© Springer-Verlag GmbH Germany, part of Springer Nature 2023

## Abstract

In the present work, geological and geotechnical studies were carried out to find the causes and mechanisms of a reinforced embankment slope failure. The information collected from the surface investigations combined with the borehole data analysis helped to understand the landslide process, to perform analyses to determine the movement mechanism, and to identify the factors contributing to the landslide. Subsurface features, including the sliding mass, slid surface, stable layer below slid surface, and groundwater, are determined based on borehole logs, from which cores of landslide masses and bedrock have been retrieved and analyzed. Laboratory tests were carried out to estimate the geomechanical properties of soil, sandstone, and mudstone that constitute the slope. Slope stability analyses were carried out to evaluate the effectiveness of the reinforcement system and to analyze the failure mechanism. A discussion is presented on the following aspects: (a) influencing factors and failure mechanism and (b) synergistic effect of rainfall and weak layer. The results show that the rainfall is the main inducing factor of slope instability, while the effect of the groundwater on the weak layer played a vital role in the landslide event. The anti-slide pile structure was found to be damaged, which indicates that further research is required in coming up with better designs and constructions of such structures for high fill slopes with soft foundations. The results also indicated that an effective drainage system should be implemented in improving the stability of the slope.

**Keywords** Embankment slope · Reinforced slope · Reactivated landslide · Weak layer · Rainfall

## Introduction

Landslides are one of the most serious geological hazards throughout the world. There are numerous studies on the triggering mechanisms of landslides across the world. It appears that landslides are complex phenomena that result from an interaction of numerous factors: geological, geomorphological, physical, and human. These factors often act together to cause a slope failure, and most of the time it becomes difficult to assess the prominent factor causing instability in an area.

For internal factors, most researchers have focused on the failure mechanisms of weak interlayers (Ronchetti et al. 2009; Di Maio and Vassallo 2011; Regmi et al. 2013; Grana and Tommasi 2014; Alonso and Pinyol 2015; Zhao et al. 2019; Liu et al. 2020; Zhang et al. 2022; Zhang and Wang 2023). Many studies have attempted to find ways of correlating landslide occurrence with precipitation (Hong et al. 2005; Montrasio et al. 2011; Kuo et al. 2013; Bai et al. 2014; Zêzere et al. 2015; Yi et al. 2021; Bourenane et al. 2022; Li et al. 2023). The research on this topic presents a clear tendency for landslide occurrence to increase with increased rainfall, whereas the critical precipitation that triggers the slope failure mostly depends on a change in the groundwater conditions (Casagli et al. 2006; Schulz et al. 2009; Wu et al. 2014; Sun et al. 2019; Sun et al. 2023), which result in increasing the weight of the saturated materials and increasing the pore-water pressure and thus decreasing the effective stress and hence the strength of the materials (Matsuura et al. 2008; Vassallo et al. 2015; Kang et al. 2020; Peng et al. 2022).

✉ Qiuxiang Huang  
qiuxiang.huang@foxmail.com

<sup>1</sup> State Key Laboratory of Geohazard Prevention and Geoenvironment Protection (SKLGP), Chengdu University of Technology (CDUT), Chengdu 610059, China

<sup>2</sup> Rock Mass Modeling and Computational Rock Mechanics Laboratories, University of Arizona, Tucson, AZ 85721, USA

Human activity has been recognized as an important triggering factor that leads to many landslides (Husein Malkawi and Taqieddin 1996; Wasowski 1998; Kang et al. 2009; Wei et al. 2012; Taga et al. 2015; Maduka et al. 2017; Hu et al. 2019; Huang et al. 2020; Yu et al. 2021; Huang et al. 2022). Filling requirements are often encountered in the construction of airports, highways, and railways in mountainous areas. The quality of the embankment is greatly influenced by the subgrade materials, the general geology of the area, and the materials used for construction. The stability of the embankment also depends on the construction method and drainage system, coupled with some external factors such as rainfall, earthquakes, dynamic traffic load, and reservoir water (Al-Homoud et al. 1994; Kamai and Sangawa 2011; Proutzopoulos et al. 2014; Alonso and Pinyol 2015; Tandon et al. 2021; Shinoda et al. 2022).

In addition to the complex and variable geological conditions and environmental conditions, the lack of understanding of embankment failure mechanism and the imperfection of current stability design methods are also the main reasons for the failure of filled subgrade slopes. The present study

deals with a complex landslide that occurred in a reinforced embankment slope through a reactivated ancient landslide. Geological and geotechnical studies were carried out to find the causes and mechanisms of failure.

## Setting

### Overview of the landslide development history

On October 3, 2009, at about 15:20, a complex landslide occurred in Panzhihua, Sichuan province of China, on the east side of the runway in Panzhihua airport (see Fig. 1). The landslide area (Fig. 1b) can be separated into two sections, the embankment slid area and the reactivated ancient landslide area located at the lower part of the embankment slope, with an estimated volume of about  $5.1 \times 10^6 \text{ m}^3$ . This failure resulted in considerable damage to the runway of the airport and led to the interruption of Panzhihua airport.

As revealed by previous investigation results, a part of the study area originally belonged to an ancient landslide

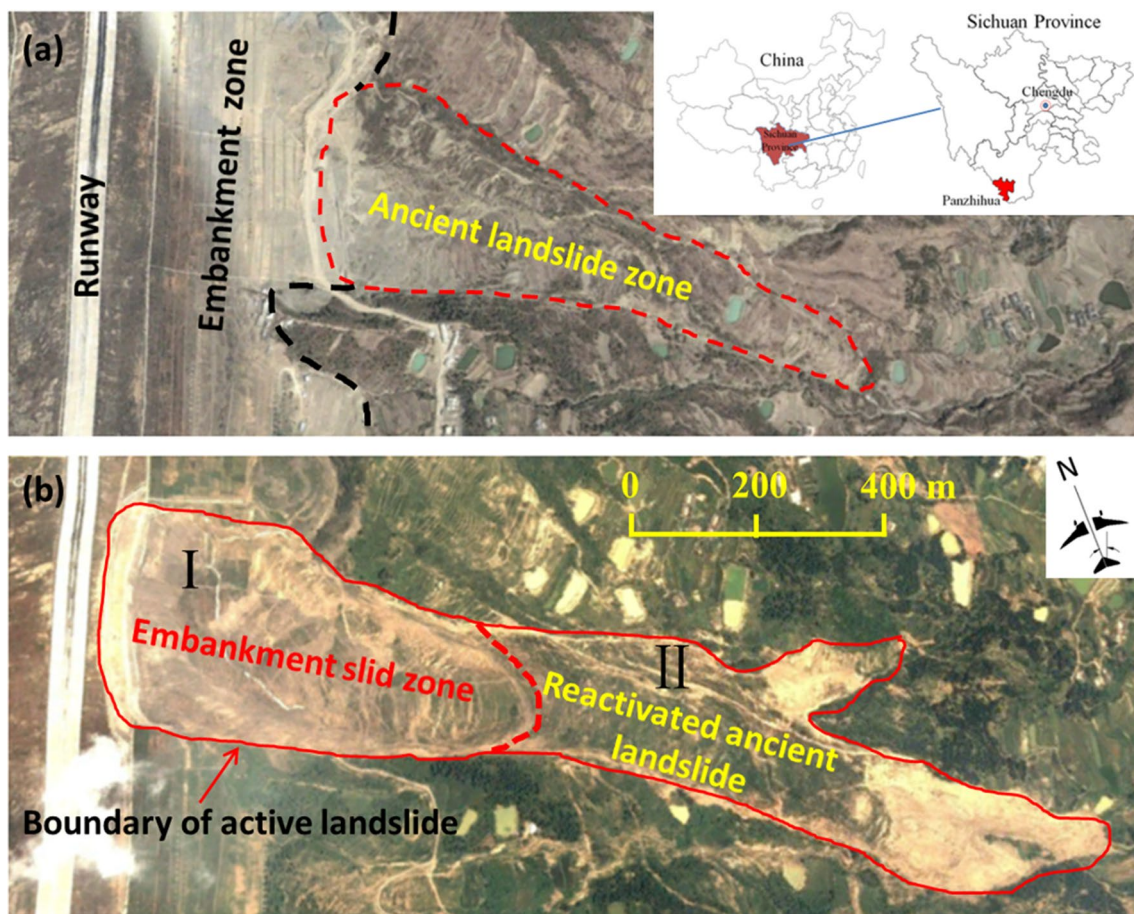


**Fig. 1** Pre- and post-failure Google images of the study area; inset maps show the general location of the landslide in China. **a** Google image of pre-failure, obtained in April 2009. **b** Google image of post-failure, obtained in Sep. 2010

**Table 1** The landslide development history

Time	Event
Jan. 2001	Cracks developed in the embankment zone.
July 2002	The slide occurred at the foot of the embankment slope; then, 3 lines of anti-slide piles were installed.
Aug. 2008	Visible cracks developed in the embankment zone after an earthquake occurred on 30th Aug.
Oct. 2009	The filled zone lost stability; the YJP landslide was simultaneously reactivated.

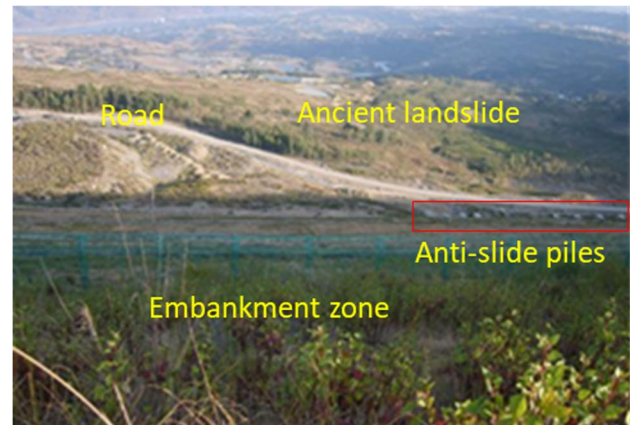
**Fig. 2** Anti-slide piles exposed after a slide occurred in July 2002 (mirror to upslope)

(named as YJP landslide hereafter). It was in stable condition before the airport construction. The aforementioned instability framework was the result of a complex evolution, characterized by instability phenomena with different extensions and evolutionary stages, as given in Table 1.

The embankment construction began in 2000. During the construction process, loose deposits (including some ancient landslide deposits) on the surface of the original slope of the runway area were removed and then filled and compacted layer by layer, and finally, anti-slide piles were installed at the foot of the embankment slope.

Possibly influenced by the construction, the YJP landslide began creeping with bulging developing in the upper slope part, coincident with cracks appearing in the embankment area, in January 2001. The opening of new fractures on the slope enabled infiltration of rainfall into the slope body resulting in softening and weathering of the sliding mass and a decrease in shear strength. This, was coincident with a rise in precipitation, resulting in a slide at the foot area of the embankment slope about 300 m in width, in July 2002. This instability damaged the constructed anti-slide piles as shown in Fig. 2.

To protect the embankment slope, stabilization works, including a retaining structure (3 lines of anti-slide piles) and a drainage system (two concrete drainage ditches),

**Fig. 3** Contact relation between the embankment slope and the YJP landslide before failure occurred (mirror to downslope)

were constructed in 2002. Two lines of anti-slide piles were installed at the middle-lower part of the embankment slope, while the third line of the anti-slide piles was installed at the toe area. The two drainage ditches were installed on both sides of the slope to reduce the surface water infiltration into the slope body. Hence, the slope became stable again. The contact relation between the embankment slope and the YJP landslide is shown in Fig. 3.

The embankment slope resumed activity in 2008. An earthquake of magnitude 6.1 occurred at 16:30 h on 30 August 2008 in Panzihua with an epicenter of 26.2° N and 101.9° E, located at 35 km from the airport. The earthquake resulted in crack development in the embankment slope, leading to a sharp decrease in the strength of the man-made fill material. Serious instability phenomena were observed in the zone located on the east side of the runway during the rainy period of 2009 as revealed by the field investigations and displacement analyses (described in the following sections).

After a few such movements of the filled zone, the overall instability of the embankment slope occurred on October 3, 2009, with sliding mass depositing on the upper part of the YJP landslide. This led to the reactivation of the YJP landslide. Hereafter, we refer to the two slides as zone I and zone II sections (see Fig. 1b) of the landslide, which is the research object of this paper.

### Geographical and geological setting of the study area

As mentioned before, the YJP landslide was in stable condition before the airport construction, with a gentle slope gradient of 8–10°. Many gullies developed on the slope body, and ponds of varied sizes were scattered in the middle and lower part of the slope (Fig. 4a). The embankment zone for the runway area construction was

located at the upper part of the ancient landslide, with a region of 3.5km length in the N-S, 0.7km width in the E-W. The runaway area was at an elevation of 1976 m, while the embankment slope was located on its east side. After the embankment construction, the gradient of this slope part turned out to be 25–26° compared to the original value of 10–18°, with a maximum thickness of filled zone up to 50 m and a slope height of 150 m (see Fig. 4b).

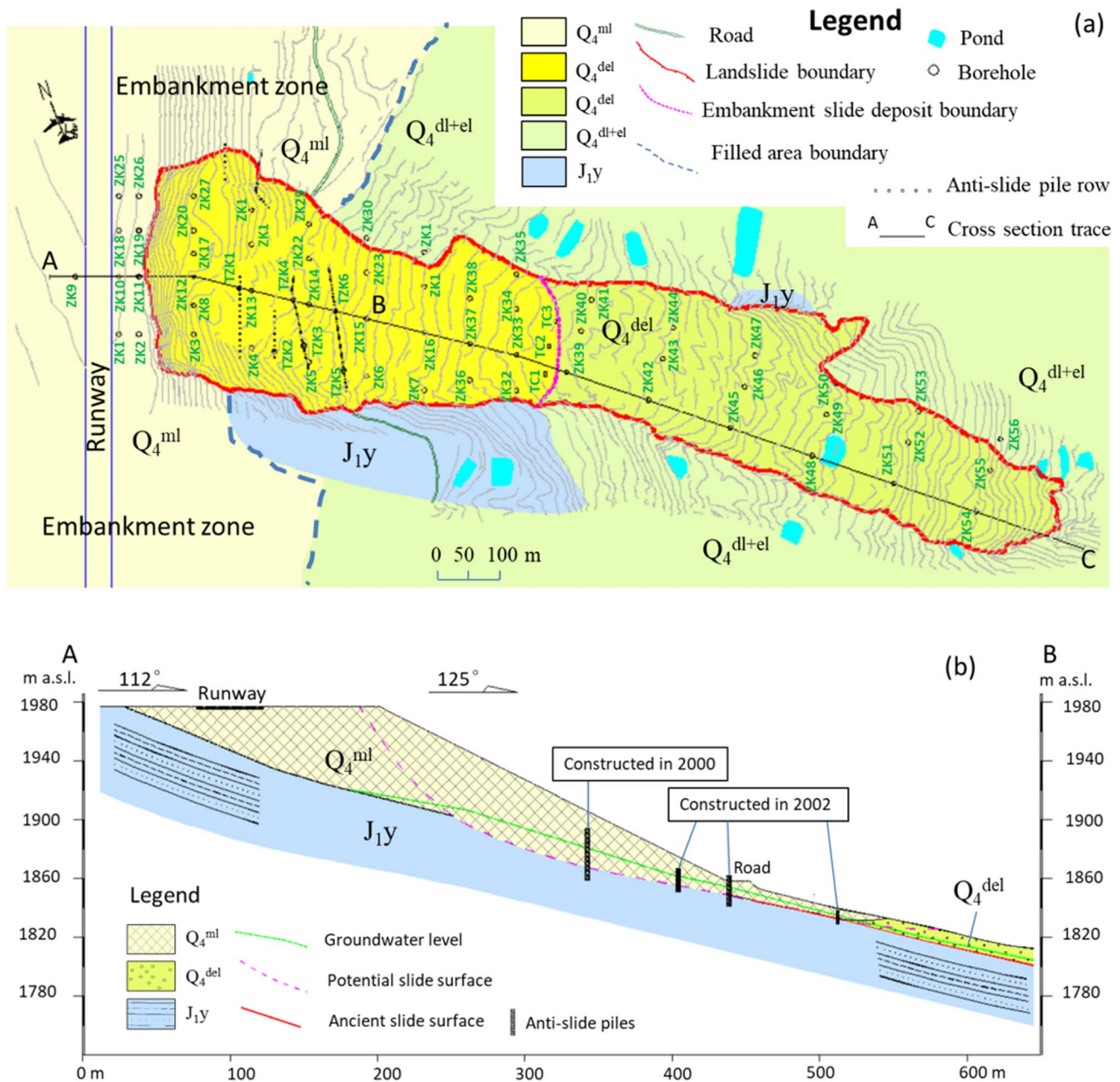


**Fig. 4** Geological and geotechnical setting of the study area. **a** Detailed geologic map of the study area. Also shown are the original locations of the anti-slide piles before failure and the locations of the

boreholes set for the field investigations. **b** A pre-failure cross-sectional profile of the embankment slope

The geological environment of the region is dominated by the Quaternary and the Yimen group of Lower Jurassic ( $J_{1Y}$ ), almost mantled quaternary material, as shown in Fig. 4a.

- The quaternary materials ( $Q_4$ ) involved in the landslide were mainly composed of three units, including the man-made fill material ( $Q_4^{ml}$ ), landslide deposits ( $Q_4^{del}$ ), and alluvial deposits ( $Q_4^{dl+el}$ ).
  - The man-made fill material ( $Q_4^{ml}$ ) mainly appears in the embankment zone for flight runway construction, with thickness ranging between 8 and 50 m. This unit was primarily composed of grayish-yellow and yellowish-brown talus debris generated from strongly to moderately weathered sandstone and mudstone.
  - The thickness of the landslide deposits of quaternary material ( $Q_4^{del}$ ) varied between 12 and 25 m. This unit was mainly composed of yellowish-brown silty clay, interspersed with strongly weathered rock fragments generated from sandstone and mudstone.
  - The alluvial deposits ( $Q_4^{dl+el}$ ) spread over the slope on both flank sides of the landslide with a thickness ranging from 3 up to 10 m. This layer was made of mostly yellowish-brown, grayish-yellow silty clay, with a small percentage of grayish-white clay, and sometimes containing fragments of highly weathered sandstone and mudstone.
- The outcrop rocks in the study area belonged to formations of the Lower Jurassic. Alternating layers of carbonaceous mudstone and sandstone made up the bedrock of the slope. The carbonaceous mudstone formation was characterized by a pelitic texture, while the sandstone formation was of fine-grained texture. The stratum dipped in the direction of  $97\text{--}165^\circ$ , with an inclination of about  $8\text{--}18^\circ$ , with that of the slope.

In the study area, the mean annual temperature was about  $20.9^\circ\text{C}$ . Most of the precipitation was concentrated from June to September, accounting for about 95.5% of the year. The average annual precipitation was roughly 801.6 mm, with a maximum of 1006.9 mm. Figure 5 shows the monthly precipitation data covering 6 years (2005 to 2010) taken from the Panzhihua airport gauging station. It also shows the amount of precipitation during the rainy periods in 2009 and 2010, when the landslide phenomena in the studied sites occurred.

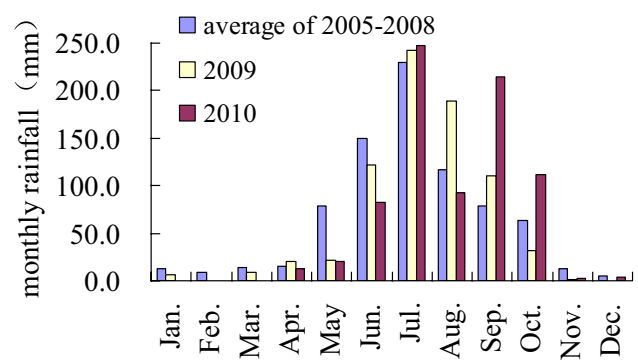


**Fig. 5** Monthly precipitations of the years 2009 and 2010 and the mean monthly precipitation for the period 2005–2008 that were recorded at the airport gauging station

## Materials and methods

To understand the processes which caused the reactivation, a series of geological and geotechnical investigations were carried out immediately after the landslide took place, in Oct. 2009.

Field investigations were carried out to obtain the slope direction, slope angle, attitude of the beds, and various deformations at different locations. To assess the subsurface conditions, 62 boreholes (see Fig. 4a for locations) were made. Among them, 56 boreholes are prefixed by ZK-, and the remaining 6 boreholes are prefixed by TZK-, which are used to detect failure of anti-slide piles. In addition, three exploratory trenches (TC1–TC3) were dug to identify the causal relationship between the embankment sliding mass and the ancient landslide.

Samples of each layer, including the embankment material, ancient landslide deposits, and bedrock involved in the landslide, were taken for laboratory testing to improve understanding of the material characteristics. Both undisturbed and disturbed samples were collected from boreholes or outcrops and cut faces at different position. All samples were packed in sample boxes and sent for testing in time.

The physical and mechanical properties of the embankment sliding zone obtained from the performed tests on samples taken from boreholes included the unit weight, porosity, natural water content, grain size distribution, and direct shear test. The samples for grain size distributions collected at seven different sites of the embankment sliding area represented different layers of the embankment body. The shear strengths were obtained from the direct shear tests conducted under both natural and saturated conditions.

Laboratory tests were carried out systematically on material from the YJP landslide zone. Landslide deposits were collected from the boreholes. The samples were predominantly obtained from the depths of the sliding zone. To determine the physical parameters of the materials, the performed tests included unit weight, porosity, natural water content, degree of saturation, and Atterberg limits. Special attention was paid in determining the shear strength on samples collected from depths where the slip surface was located. Different types of shear tests were performed on both the undisturbed and remolded samples under natural and saturated conditions, including the drained direct shear test and the repeated direct shear test to obtain the residual strength.

To characterize the geotechnical properties of the bedrocks, 10 blocks of moderately weathered sandstone and 11 blocks of moderately weathered mudstone were collected; various properties like density, deformability parameters, and shear strength parameters were determined under both the natural and saturated conditions. In addition, the softening coefficient (ratio of the uniaxial compressive strength of rock under saturated and natural state) was determined.

To evaluate the function of the reinforcement system and to analyze the failure mechanism, an embankment slope stability analysis was carried out considering the reinforcement and using the results obtained from the boreholes and field and laboratory testing. Slope stability analyses were carried out on the original cross section (before the landslide occurred, see Fig. 4b), for natural as well as saturated conditions because the slope failures occurred during the rainy period.

The data obtained from the field and laboratory investigations were analyzed to understand the landslide process and movement mechanism.

## Results

### Macroscopic deformation and movement characteristics

The wider landslide area can be separated into two sections; the upper part is the embankment sliding zone (denoted as zone I), while the lower part is the reactivated YJP landslide (referred to as zone II), as shown in Fig. 1b. From the crown (altitude about 1975 m) to the tip (altitude about 1550 m), the total length of the slope is approximately 1800 m and the width of the displaced mass is about 200–400 m, in the shape of a long tongue. The landslide mass movement was mainly in the direction of  $125^\circ$  with a displacement of 100–300 m in this direction. When combined with the borehole results, the thickness of sliding mass ranged between 10

and 25 m, and the estimated volume was found to be around  $5.1 \times 10^6 \text{ m}^3$ .

After the embankment instability occurred, rear and flank scarps could be seen clearly. The main back scarp was located at 1975 m a.s.l. with vertical movement of 30–35 m and a head width of 350 m (Fig. 6a), with a scrape of 3–5 mm, maximum value up to 20 mm in depth (Fig. 6b), while successive minor scarps with vertical movements of 5–10 m were observed within the embankment sliding zone (Fig. 6f). Rear south flank scarp had a height of 15–20 m, with bedrock outcrop as the top layer. The attitude of scarps at this position varied differently with a circular shape, having a direction ranging between  $115$  and  $135^\circ$  and an inclination changing from steep to gentle with dip angles of  $29$ – $31^\circ$  in the translational part, as shown in Fig. 6e. This type of phenomena indicated a rotational movement in the rear section of the embankment. Scarp was also obvious in the north flank. Figure 6h shows the characteristics of the scarp on the front middle part of this flank, which is 3–5 m high; the scrapes have resulted from sliding in the direction of  $175$ – $195^\circ$  with dip angles of  $6$ – $13^\circ$  and depth of 2–4 mm.

As mentioned before, the landslide body consisted of the embankment sliding zone and YJP landslide zone, with highly different movements between the two sections, for both type and rate.

Zone I is characterized by a rotational-translational movement, turning from mainly a rotational slide (in the upper part) to a translational movement (in the lower part), with a maximum displacement of sliding mass up to 300 m. The upper part of the failed embankment slid in rotational movement with severe deformation, generating a series of terraces with 30–50 m in width, 170–180 m in length, and scarps in height of 15–30 m. In the translational movement part, the lower part of zone I showed obvious flow signs (Fig. 6g), with smooth surface undulations and slope gradients of  $8$ – $13^\circ$ , and the sliding mass of this part spread downwards with deposits overlaying the zone II, YJP landslide. The maximum displacement of zone I was around 300 m. This movement destroyed anti-slide piles and it can be clearly seen in the slid body (Fig. 6g), with residue body material appearing in a borehole at depths of 7.8–10.26 m (Fig. 7). Note that this borehole was located 70 m downwards from the original location of the anti-slide piles (Fig. 4). Also, corings from boreholes TZK1–TZK6, which are used to detect failure of anti-slide piles, reveal that the anti-slide piles have been cut off. These phenomena proved that the anti-slide piles were completely destroyed.

The landslide body of zone II indicated translational movement. The upper part of zone II still maintained the overall structure of the old landslide, with a sliding distance of 130–150 m and vertical and oblique cracks on the sliding body. The lower part of zone II was the front part of the

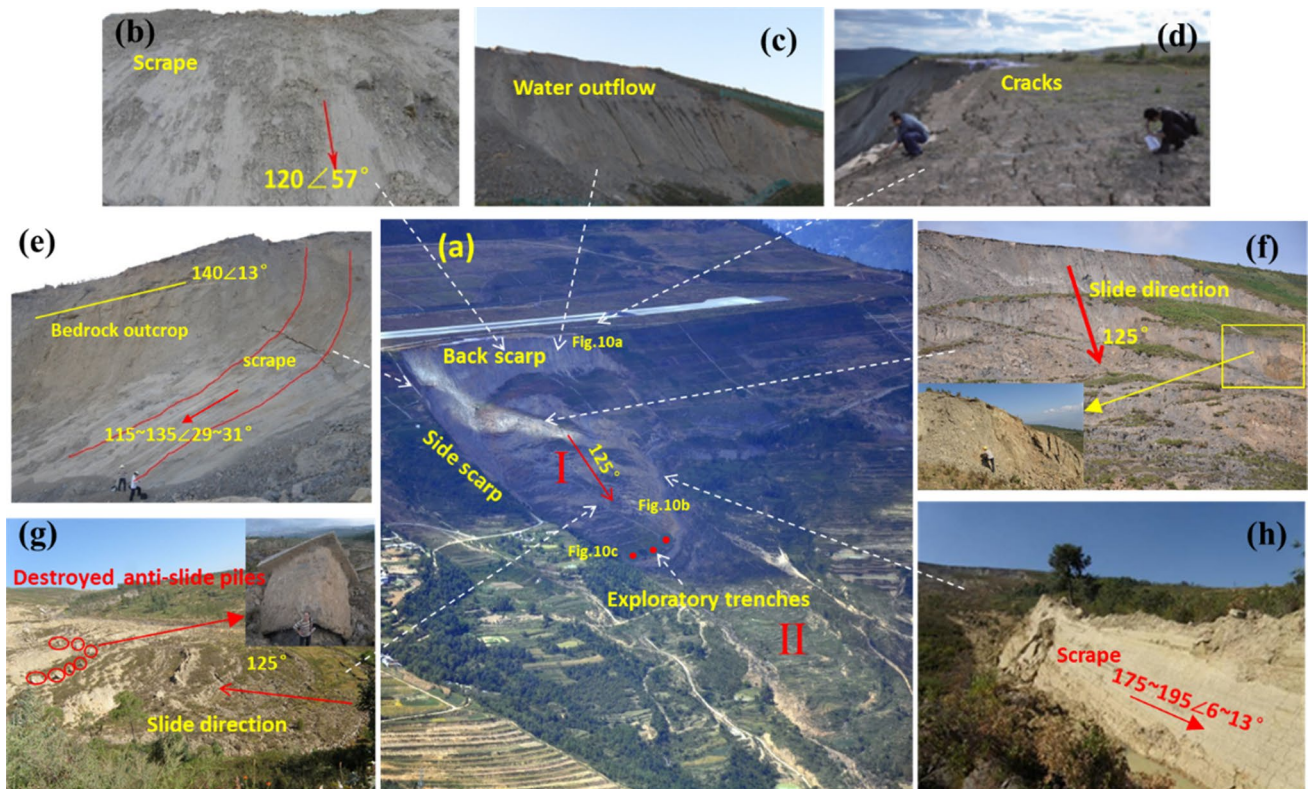


**Fig. 6** Comprehensive photos show destroyed phenomena. **a** General view of failure zones. **b** Scrape at the back scarp. **c** Water discharge at the back scarp. **d** Cracks at crown. **e** Scrape at the south flank. **f** Sec-

ondary scarps at the back part of zone I. **g** Destroyed anti-slide piles at the lower part of zone I. **h** Scrape at the north flank

**Fig. 7** Details of the borehole coring (ZK-23) showing the residue body material of the anti-slide piles; see Fig. 4a for the drilling location



landslide. Its sliding distance was 80–100 m, and the ground showed undulations with soil bulging by the extrusion. Due to the steep terrain, sliding body multi-graded disintegration and resulted in developing a secondary slide.

Moreover, outside the landslide area, influenced by the instability, a series of destructions appeared at the top of the embankment slope, in the forms of ground cracking and sinking, resulting in a crack density area about 10 m in width

near the crown area (see in Fig. 6d). The cracks developed perpendicular to the slid direction, with variable widths, from 2 to 50 cm, and variable vertical offsets from 2 to 40 cm.

**Material composition**

The field investigation, including trenching and drilling work, revealed the structure of the landslide body, including the material, thickness of each layer, and groundwater condition (Figs. 8, 9, and 10).

**Sliding mass**

Sliding body thickness of zone I ranged between 12 and 25 m, with 20–25 m at the upper part, and decreasing proceeding downwards, with ending at 12–15 m. Sliding mass of this section includes two different units, an upper layer (①, see in Fig. 8) made of embankment material (Fig. 8b) and a lower one (②, see in Fig. 8) made of grayish-yellow and yellowish-brown silty clay with fragments derived from the strongly weathered sandstone and mudstone (Fig. 8c).

**Fig. 8** Drilling work revealed the structure of the landslide body, including the material, thickness of each layer, and groundwater condition. **a** Cross section of the landslide along the trace line A-C depicted in Fig. 4a. **b–f** Typical corings showing the material of ①, ②, ③, ④, ⑤; see Fig. 4a for the drilling location. ① Man-made fill material; ② dynamically compacted grayish-yellow and yellowish-brown silty clay; ③ grayish-yellow and yellowish-brown silty clay with high water content; ④ strongly weathered mudstone; ⑤ moderately weathered mudstone and sandstone

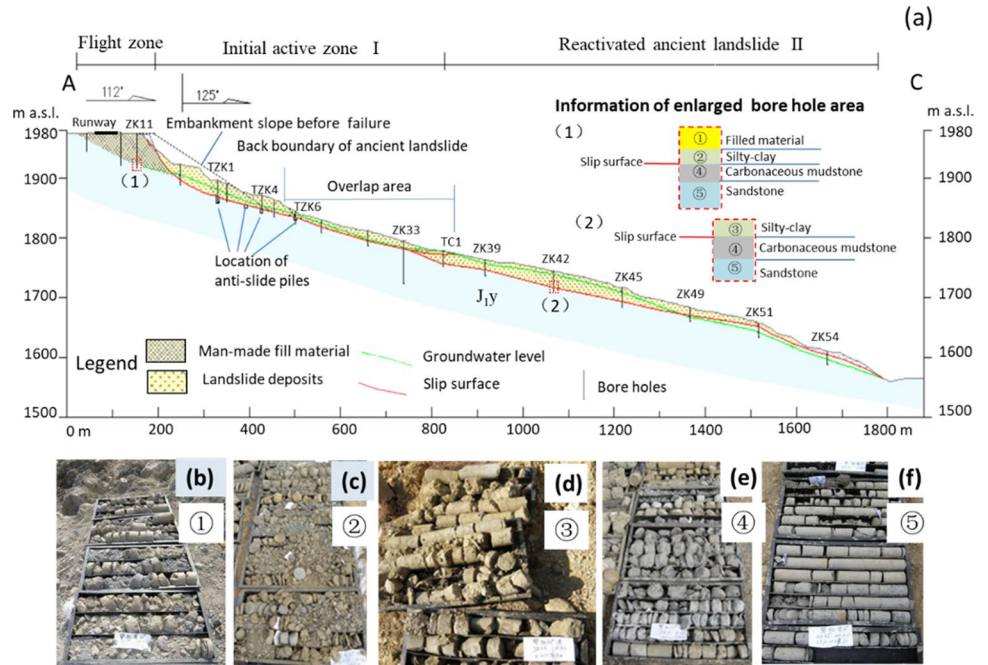


**Fig. 9** Details of the typical borehole coring and trenching showing the material and characteristics of the slip surface. **a** Morphology of slip surface revealed by drilling, text on the left side showing the depth of the slip surface. **b** Morphology of the slip surface at the front edge of zone I and shear outlet exposed by the trench

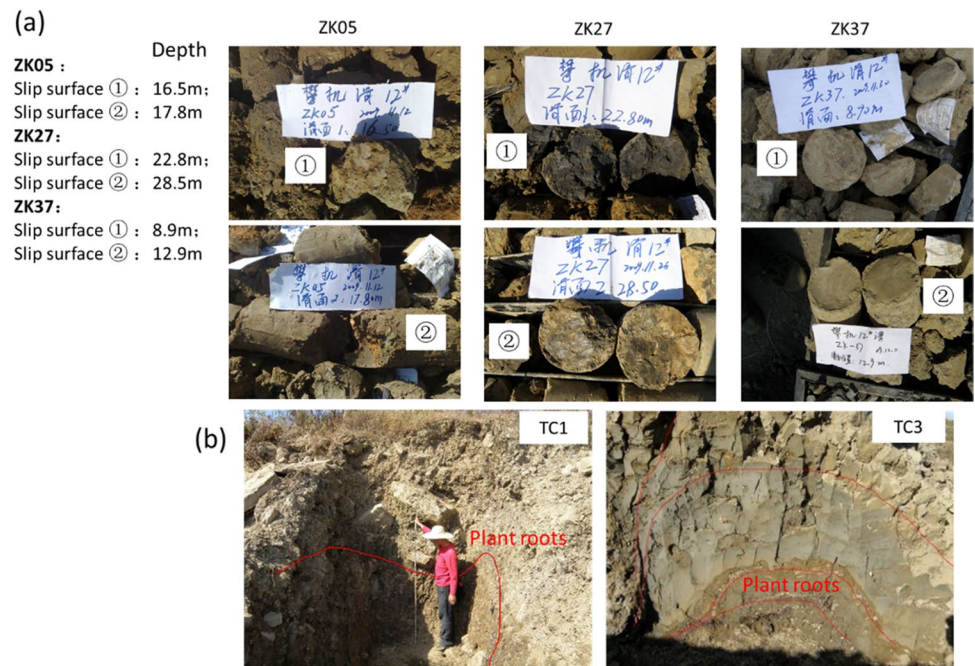






**Fig. 10** Surface water exposures observed in the landslide area during field investigations (the approximate locations are shown in Fig. 6a). **a** Groundwater outflow from part drainage holes seated in the filled

body. **b** Water pond on the north side of the landslide. **c** Water groove on the south edge of the landslide

The thickness of zone II was about 5–22 m, with 18–22 m in the upper part and 5–10 m in the lower part. The sliding mass mainly consisted of silty clay with rock fragments in percent of 10–20%, dominated by yellowish-brown strongly weathered sandstone (Fig. 8d).

It was worth noting that the material in the lower part of the embankment sliding area (zone I) is dynamically compacted silty clay, and its material composition was similar to that of the ancient landslide area (zone II), indicating that this part of the material belonged to the original slope. Moreover, most of the core drilling results showed that when the water content of the sliding mass was low, its state was close to Fig. 8c, and when the water content was high, its state is close to Fig. 8d. This is because silty clay is weak in nature, low in strength, and strong in plasticity, while the soil from the lower part had high water content, the samples were of medium-high plasticity.

### Sliding zone

With the failure of the embankment slope, the material slipped away, forming smooth walls and scratches on the rear and both flanks (Fig. 6b, e, h). These exposed sliding zones on the surface show that the thickness of the sliding zone is 10–20 cm, and the material of the sliding zone is mainly gray-yellow and yellow-brown silty clay, containing a small amount of strongly weathered sand and mudstone fragments, and the size of individual stones can reach 50 cm. The large particles contained in the sliding belt made deep scratches on the sliding surface during the sliding process.

Most of the exploration boreholes on the landslide body can clearly reveal the position of the sliding zone, which is at depth of 3–25 m, with the slip surface developed along the top of the bedrock. There are many examples of polished and slickenlined surfaces (Fig. 9a). The material of sliding zone is mainly grayish yellow and yellowish-brown silty clay with fragments of moderately-strongly weathered sandstone and mudstone, with a thickness of 10–20 cm. However, the thickness of the sliding zone in the middle-lower part of the landslide is 30–60 cm.

The results of exploratory trenches (location shown in Fig. 6a) indicated that the filled material overlaid on the landslide deposits directly, with abundant plant roots at the interface (Fig. 9b). In addition, the interface was undulating and a steeply inclined slip surface with scrape was found in the sliding body (Fig. 9a, ZK05). These types of phenomena indicated that there were secondary slid surfaces developed in the embankment sliding zone, resulting in sliding mass deposited on the landslide, while a deeper movement occurred along the ancient slid surface.

### Sliding bed

According to the borehole data, the stable layer below slip surface consisted of two different units, mudstone and sandstone, located at depth of 10–25 m from the ground surface. The material of the upper stable layer was moderately-strongly weathered carbonaceous mudstone (Fig. 8e), with a thickness of 1.5–4.0 m and a low hydraulic conductivity. The lower stable layer was moderately weathered sandstone (Fig. 8f), thick-bedded, with a thickness of over 15 m, and the rock mass was strongly jointed resulting in good water permeation.

### Groundwater

The conducted site investigations and surveys indicated that the groundwater in the landslide area was relatively developed. Several subsurface discharges of groundwater appeared on the back scarp (Fig. 6c), and water ponds in surface depressions were scattered both in and outside the sliding area (Fig. 4a). These phenomena showed that the groundwater was abundant in the areas of filled slope and the YJP landslide.

The boreholes located in the top area of the embankment slope revealed that the water level depth is about 15–16 m in the south area, while it was about 50 m in the middle area. Once in an emergency rescue project, a series of drainage

holes were made in the filled body. Some of those holes had groundwater outflow and the rest were dry holes (Fig. 10a). So, a conclusion can be made that there was no continuous water level in the filled slope body, and the groundwater was a kind of perched water, formed from direct infiltration of rainfall.

There is basically no groundwater in the rear part of the active sliding area of the filling body (ZK12, ZK13, ZK14), and groundwater begins to appear in the middle part of the sliding mass (ZK15, ZK16), and the water level is buried at a depth of about 10 m. The buried depth of the groundwater level gradually becomes shallower, and groundwater is exposed on the surface. In the low-lying areas on both sides of the landslide, groundwater leaching can be seen, forming small puddles (see Fig. 10b, c). In addition, the water depth in the YJP landslide was 5–10 m, and the groundwater level reached the surface of the slope during the heavy rainfall in the upper area.

## Geotechnical properties

Field investigation and laboratory testing to obtain geotechnical properties, which formed an important element to identify and enhance understanding of the instability phenomena.

### Embankment materials

The material was composed of yellowish-brown silty clay and fragments generated from moderately-highly weathered sandstone and mudstone. According to the particle size analyses of all samples (as shown in Fig. 11), the material in the middle and lower part of the filled body was found to be mainly composed of fine particles, with the percentage of fines higher than 50% and up to 85% with grain size smaller

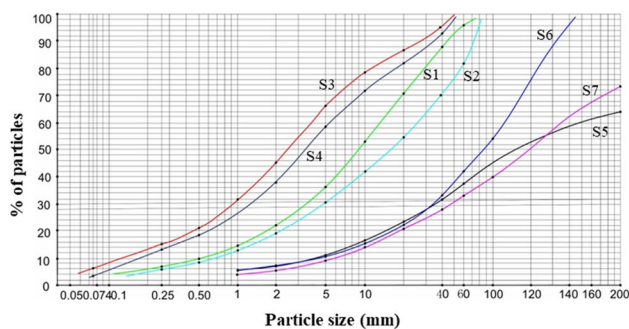


**Fig. 11** Grain size distributions of seven samples obtained from the embankment area, with four samples (named as S1–S4) collected from the back scarp area representing the material of the middle-lower part of the embankment and the other three samples (referred to as S5–S7) from the crown area representing the material of the upper part

than 20 mm. The percentage of fines in the upper part material of the filled body was found to be about 20–23%, which was dominated by coarse-grained soil with boulders occasionally observed in the size of 0.5–1.0 m.

The test results of the embankment material indicated a soil porosity ranging between 0.50 and 0.65 and a natural unit weight of 19.7 kN/m<sup>3</sup> and a saturated unit weight of 21.1 kN/m<sup>3</sup>. The direct shear tests resulted in a friction angle of 25° and cohesion of 30 kPa under the natural condition and a friction angle of 23–24° and cohesion of 22 kPa under the saturated condition.

### Landslide deposits

The landslide deposits were mainly constituted of silty clay with a low content of clay or silt. The unit weight of those ranged between 17.7 and 21.6 kN/m<sup>3</sup>. The soil porosity ranged between 0.39 and 0.85. Water content values between 2.0 and 28.0% were obtained, with the lowest values resulting for the samples close to the surface. The degree of saturation, *S<sub>r</sub>*, ranged between 13 and 100%. The soil water content results showed an increase with depth; the soil from the upper part was drier, while the soil from the lower part had high water content. The samples from the slid surface were nearly under full saturation. The majority of the analyzed samples were of medium-high plasticity.

The peak shear strength was determined by means of the standard consolidated undrained triaxial tests with constant cell pressure. A friction angle of 4–26° and an effective cohesion of 10–51 kPa were obtained for the shear strength parameters. The residual shear strength parameters were determined by repeated direct shear tests on undisturbed specimens and also on some reconstituted ones. The residual cohesion ranged between 5 and 27 kPa, and the residual friction angle ranged between 2° and 20°. The water content has a great influence on the strength.

Sampling and test results show that the upper part of the landslide soil is relatively dry, and the lower part of the soil has a large water content, and some areas are close to saturation. Silty clay is weak in nature, low in strength, and strong in plasticity, and it is easy to soften under the action of water to form a weak structural surface.

### Rock masses

According to drilling and sampling, the strongly weathered carbonaceous mudstone was grayish yellow with the core fractured into soil-like fragments, while the moderately weathered carbonaceous mudstone was gray or blueish-gray, and the core was in short columnar or fragmented (Fig. 8e). When exposed to the air, core samples of the moderately weathered ones presented quick cracking and disintegration,

caused by loss of water. The saturated compressive strength of the carbonaceous mudstone was 3–11 MPa, with an average value of 6.7 MPa. It belonged to the soft rock category, with a softening coefficient value of 0.53, indicating its poor stability and high softening susceptibility in the presence of water.

The core samples from the moderately weathered sandstone layer were mostly in long columnar form and occasionally in short columnar or fragmented form, with light yellow or grayish-white color (Fig. 8f). Due to intense fracturing, the core was highly fragmented and easy to be crushed by hand. The test results indicated that the saturated compressive strength of the sandstone ranged between 10 and 139 MPa, with an average value of 47.5 MPa and high dispersion. The main reason for the variability was the presence of fractures.

### Stability of embankment slope

As mentioned earlier, four rows of anti-slide piles were placed in the embankment slope from 2001 to 2002. During the landslide, the piles were damaged and did not play an anti-slide role. Therefore, it is necessary to study the stability of the embankment slope and the forces/stresses that acted on the piles under different conditions. Section A-B (see Fig. 4b) was selected for numerical modeling. In this simulation analysis, the material composition of the slope was simplified, by ignoring the existence of the silty clay layer between the fill body and the bedrock.

Firstly, the Swedish slices method was used to calculate the stability of the embankment slope. The calculation results provided a factor of safety (Fs) value of 1.18 under

natural conditions indicating a stable state for the filled body. Under the condition of rainfall, the parameters in the saturated state were used for calculation, and  $F_s = 0.98$  was obtained indicating an unstable state.

Then, the numerical analysis software PLAXIS was used to simulate the deformation of the filled slope and the stress in the anti-slide piles under different conditions. The PLAXIS software is a finite element method numerical simulation software based on the continuum deformation theory and small deformation erection. When the simulated object undergoes a large deformation, the divided grid will be destroyed. Therefore, in this simulation, only the simulated stress of the anti-slide piles under different working conditions is obtained, which helps to make a qualitative analysis of the failure mechanism of the landslide.

According to the principle of pile-soil interaction, the distribution form of the thrust and resistance of the piles can be calculated, and the landslide thrust borne by the piles can be obtained by integrating the thrust and resistance. The calculation model is shown in Fig. 12. Horizontal constraints are applied to the left and right boundaries, and fixed constraints are applied to the bottom. In the simulation analysis, two phases, solid and liquid, were used, and the fluid-solid coupling analysis was carried out based on Biot’s consolidation theory. The Mohr-Coulomb constitutive model was selected to represent the strength of different materials used in Fig. 12, and the seepage function and soil-water characteristic curve of rock and soil were fitted by Van Genuchten equation.

Both natural conditions and rainfall conditions were considered in the calculations, and the rainfall conditions were divided into two cases: effective drainage and poor drainage.

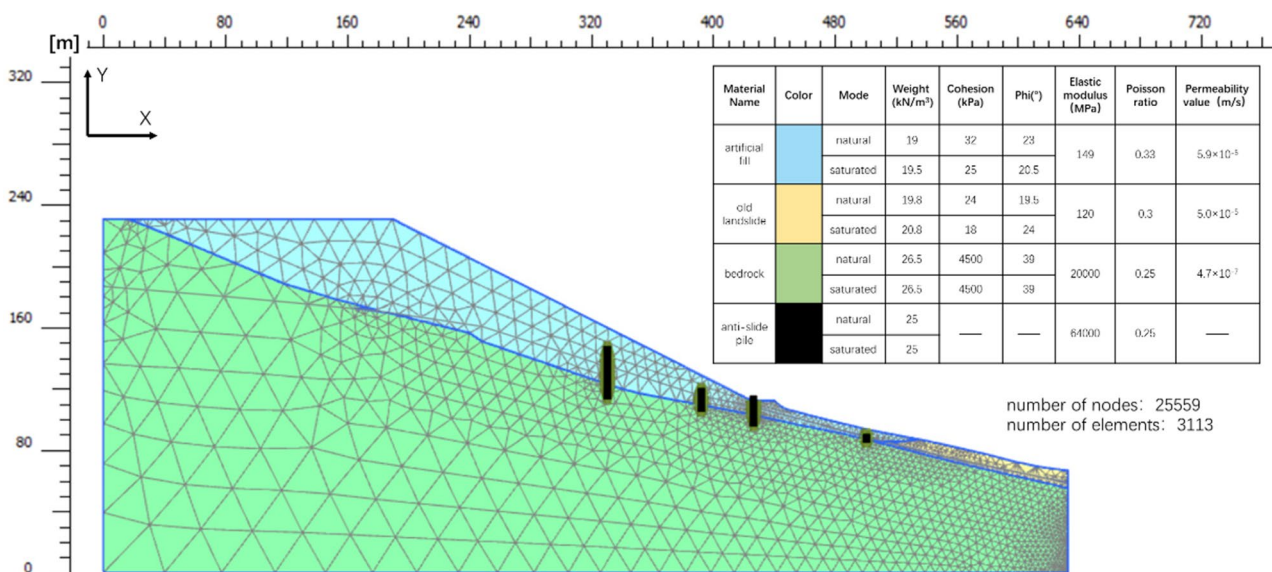


Fig. 12 The model adopted for stability analyses in PLAXIS software

Here, whether the drainage system is effective is defined in terms of the drainage effect obtained. Effective drainage means that the drainage is so effective that the groundwater level does not rise even when heavy rainfall occurs. Poor drainage means that the drainage effect is not good, and the groundwater level rises after the rainfall occurs.

Three conditions and four stages are included in the numerical simulation. Stage 1 is to simulate the initial state of the slope and initial stress generation by the K0 procedure, a special calculation method available in PLAXIS. In the subsequent simulation stages, the role of groundwater is achieved through the fluid-solid coupling function of PLAXIS, and the impact of rainfall on groundwater level is achieved by setting water boundary conditions on the surface of the slope. Stage 2 simulates the natural working condition, stage 3 simulates the rainfall condition with effective drainage, and stage 4 simulates the rainfall condition with poor drainage. The simulated stress of the anti-slide piles under different working conditions is obtained.

Case 1: the calculation results under the natural condition show that the deformation mainly occurs in the interior of the filled section, and a high deformation is distributed around the top of the fill slope (see Fig. 13a). The calculation result of landslide thrust borne by the first row of anti-slide piles is 4113 kN/m. According to the design data, the design capacity of anti-slide piles is 5000 kN/m; so the force on the pile body is less than the design standard, and the slope is in a stable state.

Case 2: under the condition of rainfall, when the drainage is effective, the influence of the groundwater only includes the saturation effect on the fill material, which increases the sliding force of the fill slope. The results show that the deformation distribution is similar to the natural condition, but the deformation is a little higher (see Fig. 13b). The calculation result of the landslide thrust borne by the first line of anti-slide piles is 5734 kN/m, which is greater than its design capacity value. Therefore, the anti-slide piles are at risk of being broken.

Case 3: under the condition of rainfall, when the drainage is poor, it includes the softening effect of the groundwater. The strength parameter values at the foundation cover interface are reduced by a reduction coefficient of 0.67. Under this condition, the landslide thrust borne by the first line of anti-slide piles is 13,714 kN/m, which is close to three times the design capacity. At this condition, it can be considered that the first line of anti-slide piles is damaged. According to the displacement distribution (see Fig. 13c), the deformation area of the slope is consistent with the actual sliding part observed in the field.

According to the above results, it can be concluded that under the natural condition, the anti-slide piles provide sufficient resistance for the filled slope, and the slope is in a stable state. Under rainfall conditions, when the drainage is unobstructed, the distribution characteristics of the slope deformation are similar to those under natural conditions. It

can be concluded that if the drainage conditions are good, it reduces the impact of the groundwater and does not form a sliding surface. However, the thrust borne by the first row of piles is greater than the design capacity. If the situation worsens, the piles are at risk of damage. In case of poor drainage, the thrust borne by the first row of anti-slide piles is far greater than its design capacity, which leads to the destruction of the first row of anti-slide piles and results in the gradual increase of the sliding force of the slope. Therefore, the fill body fails progressively, the anti-slide piles get damaged row by row, and finally, a sliding surface is formed at the foundation cover interface, resulting in the overall sliding of the fill slope.

## Analyses and discussion

### Influencing factors and failure mechanism

The instability of the slope is the result of a combination of various factors. The results of the comprehensive field investigations, laboratory tests, and stability analysis show that the formation of the landslide, in this case, is closely related to factors such as the structure of the slope, the characteristics of the rock and soil, groundwater, earthquakes, and rainfall.

The original geomorphology of the study area was a deep trough and valley controlled by the ridge bedrock. It was easy to collect the surface water and the water seeping through the bedrock. The groundwater not only softens the weak rock formations but also generates a certain amount of hydrostatic pressure and hydrodynamic pressure, which affects the stability of the slope.

Before the occurrence of the landslide, the slope gradient of the filled slope was 26–27°, which was conducive to the occurrence of the landslide. The weak layer of the carbonaceous mudstone or silty clay, which was between the bedrock and the overburden of the filled slope, was the internal cause of the landslide. This kind of weak layer has a low shear strength, and the carbonaceous mudstone is a waterproof layer. It is easy to accumulate groundwater near the interface between the bedrock and overburden, and the softening effect of the groundwater further reduces the shear strength of the weak layer. Under the control of the weak layer, the high-filled body was prone to deform and damage integrally along this interface.

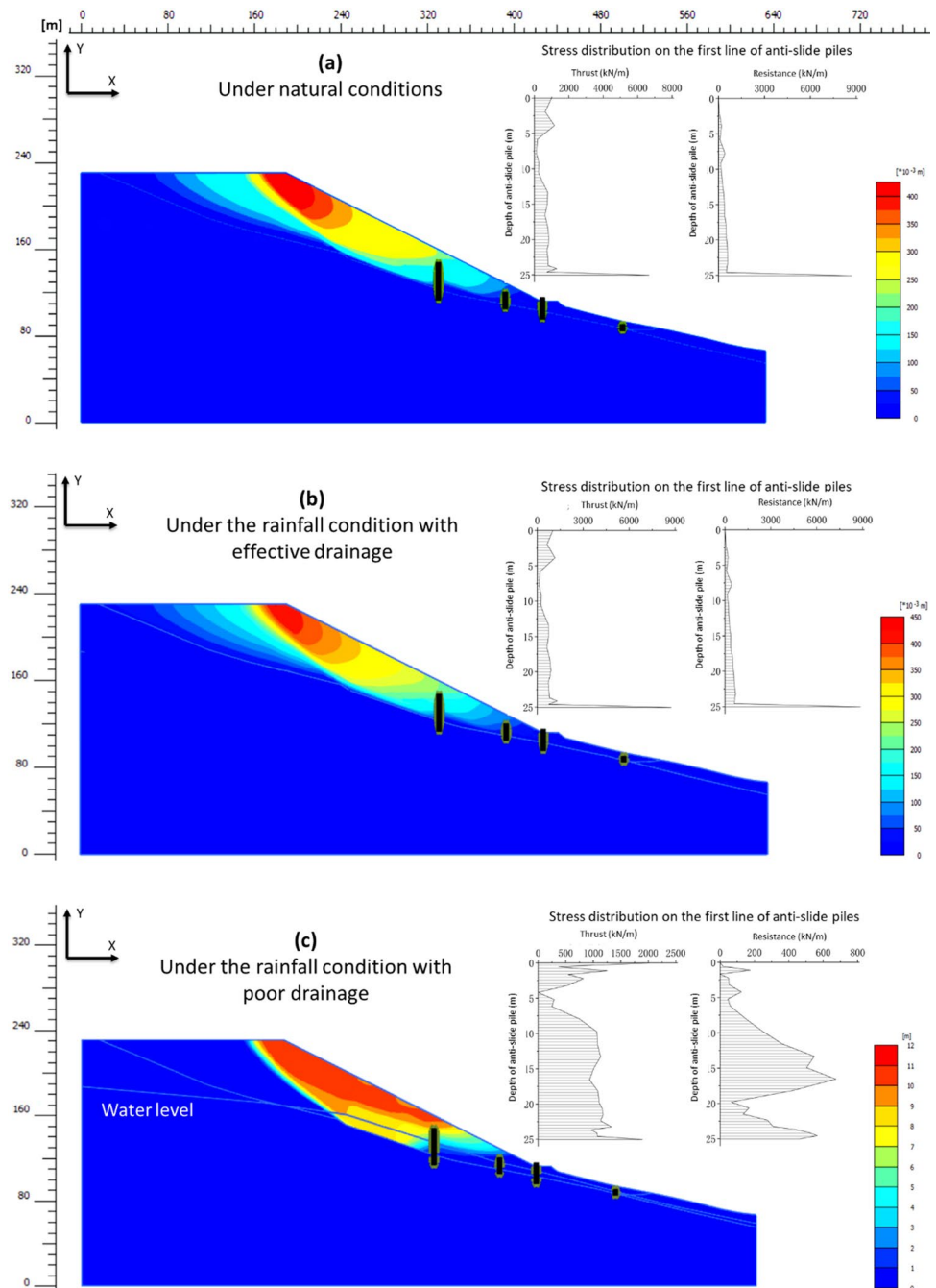
As mentioned before, an earthquake of magnitude 6.1 occurred on August 30, 2008, which caused large deformations of the high-fill slope and obvious downward staggered cracks on the slope of the soil area. Since then, the slope deformation had gradually increased, indicating that the earthquake dynamics caused certain damage to the slope, which became one of the inducing factors for the evolution of the filled slope to a landslide.

The cracks in the filling body caused by the earthquake provided a good channel for the infiltration of rainwater. This phenomenon reduced the strength of the soil body, and the filled body entered an accelerated creeping stage in the rainy season. Around the end of September 2009, there were two consecutive rainstorms. Due to that the groundwater level and water pressure in the filled body increased rapidly, and the shear strength of soils decreased. Under the combined action of the slope self-weight, pore water pressure, and seepage pressure, the thrust of the slid-filled body on the anti-slide piles exceeded the resistance that the anti-slide piles could

bear and resulted in the failure of the piles. This led to a reduction of the support for the filled body and propagation of the sliding surface and overall failure of the filled body and the anti-slide pile system. The sliding mass of the filled slope covered and pushed the ancient landslide which was located below, resulting in the reactivation of the ancient landslide.

According to the slope structure and failure characteristics, the landslide studied can be categorized as a large push type “slip pull crack” bedding landslide produced in high fill, and an old landslide, in which the filled area belongs to the active part and the YJP landslide belongs to the passive

**Fig. 13** The numerical calculation results show displacement distribution and the stress distributions of the first line of anti-slide piles under different conditions



part. As for the evolution process, firstly, the filled slope produced integral creep deformation along the interface between the foundation and overburden. With the gradual increase of creep deformation, the anti-sliding structures failed one by one, leading to the propagation of the sliding surface. Under the occurrence of the rainstorm, the high slope of the filled body produced overall instability and sliding, which induced the activation of the YJP landslide, and finally formed a complex landslide.

### Synergistic effect of rainfall and the weak layer

The instability of the filled slope is a complex one. Generally speaking, the influencing factors mainly include the following three aspects: the engineering characteristics of the fill material itself, the engineering characteristics of the underlying strata, and the interaction between the fill body and underlying strata under the synergistic action of multiple factors.

According to the structural characteristics of the filled slope, the sliding surface might have developed at the following contact surfaces: (a) the contact surface between the foundation and the filled body, (b) the contact surface between the bedrock and the overburden of the original slope, and (c) a weak layer at a certain depth of the original slope.

As mentioned earlier, the interface between the bedrock and filled body was a layer of dynamically compacted silty clay with a thickness of 3–10 m, mostly residual deluvial soil, strongly weathered sand, and mudstone of the original slope. The top surface of the bedrock was grayish black carbonaceous mudstone with a thickness of 5–15 m. Due to the great difference in strength between the Quaternary overburden and bedrock, the contact zone between the silty clay layer and bedrock becomes a relatively weak layer, which controlled the stability of the filled slope.

Rainfall was the main inducing factor of the slope instability. Rainfall infiltration increased the self-weight of the slope, led to more groundwater seepage pressure, and reduced the shear strength of the soil. The test results show that the silty clay has poor physical and mechanical properties, low strength and strong plasticity, and susceptibility to softening under the action of water. The underlying carbonaceous mudstone was a relatively impermeable stratum. The trapped water on the surface of the carbonaceous mudstone sharply reduced the shear strength of the interface between the slope alluvium and carbonaceous mudstone. Under the softening action of the groundwater, the shear strength further decreased, resulting in a change from a hard plastic state to a soft plastic or even flow plastic state, leading to large plastic deformation occurring under the action of gravity. In the case of a rainstorm, a large amount of surface water infiltrated into the slope in a short time causing the pore

water pressure in the slope to increase rapidly and inducing the filled body that has entered the stage of accelerated creep deformation to lose stability.

From the above analysis, it can be seen that the weakening effect and mechanical effect of the groundwater on the weak layer played vital roles in the whole landslide event. Therefore, during the construction of the filled body project, the slope deposit on the foundation surface should be completely removed to avoid the existence of a weak layer. At the same time, an effective drainage system should be placed in the treatment project.

### Conclusions—lessons learned

The landslide case studied in this paper is a complex landslide formed from a reinforced embankment slope and an ancient landslide. The high-filled slope slid first, and the sliding mass covered the ancient landslide located below, making it passively reactivated, thus forming a giant push-type landslide.

The rainfall is the main inducing factor of slope instability. The weak and slippery carbonaceous mudstone layer located near the interface between the foundation and overburden at the bottom of the fill was the internal cause of the landslide. The long-term softening and mechanical action of the groundwater played vital roles in the whole landslide event, which indicates the importance of an effective drainage system for the stability of this kind of slope.

During the landslide, the anti-slide piles got damaged. The stability analysis showed that the anti-slide piles had to bear a high thrust under the rainfall conditions, and the earth pressure on the first row of piles was about three times that under the natural conditions, which was far greater than the design capacity of piles. The pre-reinforced piles broke progressively from back to the front row by row, indicating that the design layout plan and determination of the stresses on the multiple rows of anti-slide piles on the fill slope were unsatisfactory.

Our lessons from the case study are the following: (a) In high filled slope engineering, special attention should be paid to the removal or treatment of the weak layer that exists at the bottom of the filled body. (b) The groundwater has a great impact on slope stability, so effective measures should be taken to eliminate its influence. (c) The design and layout of the pre-reinforced structure should be determined incorporating the possible deformation mechanism of the slope.

**Acknowledgements** The first author would like to thank the SKLGP and CDUT for providing a scholarship to conduct a part of the reported

research at the University of Arizona as a Visiting Scholar. The authors thank Liu Ji and Gu Shengzao for performing the field investigations.

**Funding** This research was financially supported by the Research Foundation of SKLGP (No. SKLGP2015Z014).

## Declarations

**Competing interests** The authors declare no competing interests.

## References

- Al-Homoud AS, Saket SK, Husein AI (1994) Investigation of failure of highway embankment founded on colluvium and suggested stabilization measures for reconstruction. *Eng Geol* 38(1-2):95–116
- Alonso EE, Pinyol NM (2015) Slope stability in slightly fissured claystones and marls. *Landslides* 12(4):643–656
- Bai S, Wang J, Thiebes B et al (2014) Analysis of the relationship of landslide occurrence with rainfall: a case study of Wudu County, China. *Arab J Geosci* 7(4):1277–1285
- Bourenane H, Bensalem R, Oubaiche EH et al (2022) The large deep-seated landslide induced by the March 12th, 2012 rainfall event in the city of Azazga, Northern Algeria: deformation characteristics and failure mechanisms. *Environ Earth Sci* 81(19):476
- Casagli N, Dapporto S, Ibsen ML et al (2006) Analysis of the landslide triggering mechanism during the storm of 20th–21st November 2000, in Northern Tuscany. *Landslides* 3(1):13–21
- Di Maio C, Vassallo R (2011) Geotechnical characterization of a landslide in a Blue Clay slope. *Landslides* 8(1):17–32
- Grana V, Tommasi P (2014) A deep-seated slow movement controlled by structural setting in marly formations of Central Italy. *Landslides* 11(2):195–212
- Hong Y, Hiura H, Shino K et al (2005) Quantitative assessment on the influence of heavy rainfall on the crystalline schist landslide by monitoring system—case study on Zentoku landslide, Japan. *Landslides* 2(1):31–41
- Hu G, Liu M, Chen N et al (2019) Real-time evacuation and failure mechanism of a giant soil landslide on 19 July 2018 in Yanyuan County, Sichuan Province, China. *Landslides* 16(6):1177–1187
- Huang QX, Xu XT, Kulatilake PHSW et al (2020) Formation mechanism of a rainfall triggered complex landslide in southwest China. *J Mt Sci* 17(5):1128–1142
- Huang X, Wang L, Ye R et al (2022) Study on deformation characteristics and mechanism of reactivated ancient landslides induced by engineering excavation and rainfall in Three Gorges Reservoir area. *Nat Hazards* 110(3):1621–1647
- Husein Malkawi AI, Taqieddin SA (1996) Geotechnical study of landslides resulting from a highway construction in Jordan. *Nat Hazards* 13(1):1–15
- Kamai T, Sangawa A (2011) Landslides on ancient embankments in the Kinki district (Japan): strong motion seismoscope of the 1596 Keichou-Fushimi earthquake. *Quat Int* 242(1):90–105
- Kang GC, Song YS, Kim TH (2009) Behavior and stability of a large-scale cut slope considering reinforcement stages. *Landslides* 6(3):263–272
- Kang X, Xu G, Yu Z et al (2020) Experimental investigation of the interaction between water and shear-zone materials of a bedding landslide in the Three Gorges Reservoir Area, China. *Bull Eng Geol Environ* 79:4079–4092
- Kuo YS, Tsai YJ, Chen YS et al (2013) Movement of deep-seated rainfall-induced landslide at Hsiaolin Village during Typhoon Morakot. *Landslides* 10(2):191–202
- Li Y, Xue K, Zhao Y et al (2023) Study on the stability and disaster mechanism of layered soil slopes under heavy rain. *Bull Eng Geol Environ* 82(7):272
- Liu J, Xu Q, Wang S et al (2020) Formation and chemo-mechanical characteristics of weak clay interlayers between alternative mudstone and sandstone sequence of gently inclined landslides in Nanjiang, SW China. *Bull Eng Geol Environ* 79:4701–4715
- Maduka RI, Igwe O, Ayogu NO et al (2017) Geotechnical assessment of road failure and slope monitoring along Nsukka-Adoru-Idah highway, Southeastern Nigeria. *Environ Monit Assess* 189(1):1–18
- Matsuura S, Asano S, Okamoto T (2008) Relationship between rain and/or meltwater, pore-water pressure and displacement of a reactivated landslide. *Eng Geol* 101(1-2):49–59
- Montrasio L, Valentino R, Losi GL (2011) Towards a real-time susceptibility assessment of rainfall-induced shallow landslides on a regional scale. *Nat Hazards Earth Syst Sci* 11(7):1927–1947
- Peng T, Chen N, Hu G et al (2022) Failure mechanism of Dege landslide in western China, March, 2021: the loess interlayer and multiple water resources. *Landslides* 19(9):2189–2197
- Proutzopoulos G, Fortsakis P, Seferoglou K, Chrysochoidis F, Vassilopoulos I, Perleros V (2014) Assessment of Failure Mechanism and Rehabilitation of a Landslide Within Marly Formations in NW Greece: From the Site Investigation to the Geotechnical Design. *Geotechnical and Geological Engineering* 32(6):1485–1502. <https://doi.org/10.1007/s10706-014-9729-8>
- Regmi AD, Yoshida K, Nagata H et al (2013) The relationship between geology and rock weathering on the rock instability along Mugling–Narayanghat road corridor, Central Nepal Himalaya. *Nat Hazards* 66(2):501–532
- Ronchetti F, Borgatti L, Cervi F et al (2009) Hydro-mechanical features of landslide reactivation in weak clayey rock masses. *Bull Eng Geol Environ* 69(2):267–274
- Schulz WH, McKenna JP, Kibler JD et al (2009) Relations between hydrology and velocity of a continuously moving landslide—evidence of pore-pressure feedback regulating landslide motion? *Landslides* 6(3):181–190
- Shinoda M, Yoshida I, Watanabe K et al (2022) Seismic probabilistic risk estimation of Japanese railway embankments and risk-based design strength of soil and reinforcement. *Soil Dyn Earthq Eng* 163:107507
- Sun HY, Pan P, Lü Q et al (2019) A case study of a rainfall-induced landslide involving weak interlayer and its treatment using the siphon drainage method. *Bull Eng Geol Environ* 78:4063–4074
- Sun L, Shen F, Li C (2023) Water-induced weakening retrogressive landslides: a study on the progressive failure process and formation mechanism of trailing edge fracture surfaces. *Bull Eng Geol Environ* 82(6):201
- Taga H, Turkmen S, Kacka N (2015) Assessment of stability problems at southern engineered slopes along Mersin-Tarsus Motorway in Turkey. *Bull Eng Geol Environ* 74(2):379–391
- Tandon RS, Gupta V, Venkateshwarlu B (2021) Geological, geotechnical, and GPR investigations along the Mansa Devi hill-bypass (MDHB) Road, Uttarakhand, India. *Landslide* 18(3):849–863
- Vassallo R, Grimaldi GM, Di Maio C (2015) Pore water pressures induced by historical rain series in a clayey landslide: 3D modeling. *Landslides* 12(4):731–744
- Wasowski J (1998) Understanding rainfall-landslide relationships in man-modified environments: a case-history from Caramanico Terme, Italy. *Environ Geol* 35(2):197–209
- Wei Z, Yin G, Wang JG et al (2012) Stability analysis and supporting system design of a high-steep cut soil slope on an ancient landslide during highway construction of Tehran-Chalus. *Environ Earth Sci* 67(6):1651–1662
- Wu CH, Chen SC, Feng ZY (2014) Formation, failure, and consequences of the Xiaolin landslide dam, triggered by extreme rainfall from Typhoon Morakot, Taiwan. *Landslides* 11(3):357–367

- Yi X, Feng W, Bai H et al (2021) Catastrophic landslide triggered by persistent rainfall in Sichuan, China: August 21, 2020, Zhonghaicun landslide. *Landslides* 18:2907–2921
- Yu X, Gong B, Tang C (2021) Study of the slope deformation characteristics and landslide mechanisms under alternating excavation and rainfall disturbance. *Bull Eng Geol Environ* 80(9):7171–7191
- Zêzere JL, Vaz T, Pereira S et al (2015) Rainfall thresholds for landslide activity in Portugal: a state of the art. *Environ Earth Sci* 73(6):2917–2936
- Zhang F, Yang T, Li S (2022) Investigation on stability of large bedding slope affected by weak interlayer creep deformation. *Mech Time-Depend Mater* 27:227–250
- Zhang Z, Wang T (2023) Failure modes of weak interlayers with different dip angles in red mudstone strata, Northwest China. *Bull Eng Geol Environ* 82(5):156
- Zhao L, Li D, Tan H et al (2019) Characteristics of failure area and failure mechanism of a bedding rockslide in Libo County, Guizhou, China. *Landslides* 16(7):1367–1374

Springer Nature or its licensor (e.g. a society or other partner) holds exclusive rights to this article under a publishing agreement with the author(s) or other rightsholder(s); author self-archiving of the accepted manuscript version of this article is solely governed by the terms of such publishing agreement and applicable law.